# DEHYDRATION OF ETHANOL OVER ZEOLITES, SILICA ALUMINA AND ALUMINA: LEWIS ACIDITY, BRØNSTED ACIDITY AND CONFINEMENT EFFECTS

Thanh Khoa Phung[a], Loriana Proietti Hernández[a,b], Alberto Lagazzo[a], Guido Busca [a,*]

[a]Department of Civil, Chemical and Environmental Engineering, University of Genova, p. J.F. Kennedy 1, 16129 Genova, Italy

[b] on leave from Departamento de Termodinámica y Fenómenos de Transferencia, Universidad Simón Bolívar, AP 89000, Caracas 1080, Venezuela

* Tel: (+39) 010 353 6024, Fax: (+39) 010 353 6028, Email: Guido.Busca@unige.it (G. Busca)

*Abstract*

Ethanol dehydration was investigated over commercial H-FER, H-MFI, H-MOR, H-BEA, H-Y and H-USY zeolite samples, and alumina and silica alumina for comparison. The catalysts were characterized using FT-IR spectroscopy of the surface OH groups and of adsorbed CO and pyridine. UV-Vis, Raman and TG-DTA were applied to characterize coke, formed more on H-MOR and H-BEA. H-zeolites are definitely more active than silica alumina and alumina on catalyst weight base. The H-MOR sample is the most active but the H-MFI samples with $Si/Al_2$ ratios 280 and 50 show higher reaction rate per Al ion, H-FER and faujasites show highest ethylene yield (99.9% at 573 K). At lower temperature and higher space velocities, diethyl ether is formed with high yield (> 70 % at 453-473 K on H-BEA and H-MFI (50)). Overconversion of ethylene mainly to aromatics is observed on H-MFI (50). The different behaviour of protonic zeolites can predominantly be explained by confinement effects on the different zeolite cavities.

*Keywords: Ethanol dehydration; zeolites; silica alumina; ethylene; diethyl ether; coking.*

## 1 Introduction

Ethylene is the main primary intermediate in petrochemistry: world production capacity exceeds 143,400,000 tpy [1]. Approximately 80 % of the ethylene consumed in US, Western Europe and Japan is used for production of ethylene oxide, ethylene dichloride, linear low density and high density polyethylene [2]. Presently, ethylene is produced commercially primarily by two processes: the steam cracking of hydrocarbon fractions performed in petrochemical complexes [3] and, to a lower extent, from the separation of refinery gas mainly obtained as a byproduct of Fluid Catalytic Cracking (FCC) of heavy oils [4]. Both processes are high energy intensive with large amounts of $CO_2$ green-house gas emissions.

In the frame of a future possible organic chemistry based on renewables, a number of alternatives exist for ethylene manufacture. One of them is the MTO (Methanol To Olefins) process [5], supposing “biomethanol” (e.g. methanol produced using syngases arising from biomass gasification) is available. Alternatively, bioethanol produced by lignocellulosics could be the primary intermediate to be converted into ethylene by catalytic dehydration

$C_2H_5OH \rightarrow C_2H_4 + H_2O \qquad \Delta H_{298} = + 44.9 \text{ kJ/mol} \qquad (1)$

The reaction (1) is endothermic, but is already largely favoured thermodynamically at moderate temperatures (e.g. 473-573 K). The dehydration of ethanol to ethylene has indeed been applied at the industrial level in the sixties using aluminas as the catalysts [6,7]. Silica alumina is reported to be more active than alumina as an acid catalyst and has also been suggested for this reaction [8]. On the other hand, a number of studies reported on the high catalytic activities of different zeolite catalysts such as H-MFI, H-BEA, H-FAU, H-FER and H-MOR for ethanol dehydration [9,10,11,12,13,14,15,16,17]. The literature in the field has been recently reviewed by Zhang and Yu [18], that concluded that zeolites might be unstable for this reaction. In contrast, Fan et. al. judged they are applicable at the industrial level to produce ethylene from bioethanol [19].

Reaction (1) suffers somehow of the competition with the production of diethyl ether (DEE)

$2\ C_2H_5OH \rightarrow C_2H_5OC_2H_5 + H_2O \qquad \Delta H_{298} = -\ 25.1 \text{ kJ/mol} \qquad (2)$

which is exothermic thus also favored at low or moderate temperature. A number of mechanistic studies performed with different techniques [20,21,22,23,24,25] have been published concerning ethanol dehydration on zeolites with some disagreement between the respective conclusions.

The dehydration of ethanol is also largely used as a test reaction for surface acido-basicity characterization [26,27,28,29]. The aim of this work is to investigate the feasibility of ethanol dehydration to ethylene over different Brønsted and Lewis acidic solids, such as zeolites, silica alumina and alumina, and complete [30] the picture of ethanol dehydration mechanisms and the nature of the acidity of these solids.

## 2 Experimental.

### *2.1. Catalysts*

Catalysts properties are summarized in Table 1. Commercial zeolites in the ammonium form were calcined at 773 K for 4 hours to thermally decompose $NH_4^+$ to $H^+$ and $NH_{3(g)}$.

### *2.2. Catalytic experiments*

Catalytic experiments have been performed at atmospheric pressure in a tubular flow reactor (i.d. 6 mm) using 0.5 g catalyst (60-70 mesh sieved, to have a ratio between the particle diameter and the internal reactor diameter near 25) and feeding 7.9% v/v ethanol in nitrogen with 1.43 $h^{-1}$ WHSV (total flow rate of 80 cc/min). The carrier gas (nitrogen) was passed through a bubbler containing ethanol (96%) maintained at constant temperature (298 K) in order to obtain the desired partial pressures. The temperature in the experiment was varied stepwise from 373 K to 623 K.

Ethanol conversion is defined as usual:

$$X_{EtOH} = (n_{EtOH(in)} - n_{EtOH(out)})/n_{EtOH(in)}$$

While selectivity to product *i* is defined as follows:

$$S_i = n_i/(\nu_i(n_{EtOH(in)} - n_{EtOH(out)}))$$

where $n_i$ is the moles number of compound *i*, and $\nu_i$ is the ratio of stoichiometric reaction coefficients.

The outlet gases were analyzed by a gas chromatograph (GC) Agilent 4890 equipped with a Varian capillary column “Molsieve 5A/Porabond A Tandem” and TCD and FID detectors in series. In order to identify the compounds of the outlet gases, a gas chromatography coupled with mass spectroscopy (GC-MS) Thermo Scientific with TG-SQC column (15 m x 0.25 mm x 0.25 μm) was used.

### *2.3. Catalyst characterization*

2.3.1. Infrared (IR) spectroscopy experiments.

IR spectra were recorded using Nicolet 380 FT-IR spectrometers. Acidity measurements were taken using the pure powders pressed into thin wafers and activated in the IR cell

connected with a conventional outgassing/gas-manipulation apparatus at 773 K. The activated samples were contacted with pyridine vapor ($p_{Py}$ ~1 torr) at room temperature for 15 min; after which the IR spectra of the surface species were collected in continuous evacuation at room temperature with increasing temperature. CO adsorption was performed at 130 K (real sample temperature measured by a thermocouple) by the introduction of a known dose of CO gas inside the low temperature infrared cell containing the previously activated wafers. The sample was saturated with CO using sufficiently high CO pressure (up to 20 Torr), until the intensity of the adsorbed species has raised a maximum. IR spectra of the surface species were collected in continuous evacuation with increasing temperatures between 130 and 273 K.

2.3.2. TG-DTA experiments

TG-DTA (ThermoGravimetry - Differential Thermal Analysis) were performed using a TG-DSC Netzsch Gerätebau STA 409 (Germany), with a weight sensitivity of 0.1 mg and equipped with a Netztch410 furnace temperature controller system. For each test, about 50 mg of the sample was placed in an alumina crucible of 6 mm in diameter and then introduced inside the furnace. All the samples were analysed in the temperature interval 323–1073 K, with a nominal heating rate of 10 K/min in static air.

2.3.3. Raman spectroscopy analysis.

Raman spectra were collected over 3-5 mg of catalysts at room temperature on Renishaw microscope, performing at least 3 analyses at different positions and reducing the exposure to air for avoiding coke oxidation in case of spent catalysts. A laser of He-Ne was used at 632.8 nm focused on the sample by a microscope.

2.3.4. UV-Vis spectroscopy analysis.

UV-Vis analysis has been performed using a Jasco V570 instrument, equipped with a DR integration sphere for the analysis of spent catalysts powder. All the spectra have been recorded in air at room temperature.

## 3 Results.

*3.1 Characterization of the surface acid sites.*

To have information on the nature of the active sites involved in ethanol conversion, surface acidity characterization studies have been performed using IR spectroscopy. We used this technique to study surface hydroxyl groups and we used molecular probes to test acidity. In our previous work [30] we remarked that the use of very weak bases (such as CO) only, as probes, might be not appropriate in this case because of their much lower

reactivity and volatility with respect to the reactant molecule ethanol. The use of the less volatile and stronger base pyridine may give more reliable results. Thus we used here both probes to characterize the catalyst surfaces.

*3.1.1 IR study of the surface hydroxyl groups.*

The IR spectra of the OH hydroxyl groups (OHs) of zeolites are presented in Fig. 1. All zeolites show a sharp OH stretching band ($\nu$OH) at ca. 3740-3730 $cm^{-1}$, which is attributed to the weakly acidic terminal silanol groups located on the external surface [31]. One or more bands in the range 3650-3500 $cm^{-1}$ are also found, attributed to the bridging Si-OH-Al groups that are exclusively on the inner surface and possess a strong Brønsted acidity [31]. In the spectrum of our H-BEA sample, the $\nu$OH band of bridging Si-OH-Al groups is very weak at 3605 $cm^{-1}$, while in the spectra of H-FER, H-MFI and H-MOR the $\nu$OH band of bridging Si-OH-Al groups is well evident in the range near 3600 $\pm$ 10 $cm^{-1}$. The spectra agree with those recorded in previous studies [31,32,33]. The two faujasite zeolites have been the object of previous studies [34,35]. The spectrum of the catalyst H-USY clearly shows two OH stretching bands due to bridging hydroxyl groups at 3627 and 3563 $cm^{-1}$: the high frequency (HF) band is due to OH groups located in the supercages (3627 $cm^{-1}$), the low frequency (LF) band to OH groups located in the sodalite cages (3563 $cm^{-1}$). Their low frequency shoulders, we observe near 3600 $cm^{-1}$ and 3550 $cm^{-1}$, have been assigned to HF and LF species, respectively, interacting with residual extraframework (EF) species [36]. The spectrum of sample H-Y shows an additional split band at 3689 and 3678 $cm^{-1}$, in the region usually assigned to OH groups located on EF material, together with the band at 3606 $cm^{-1}$, possibly with several components, in the region of zeolitic hydroxyl groups. This spectrum, where the distinction of the different zeolitic OHs is difficult, is quite typical of high Al content H-FAU zeolite [37].

Some absorption in the range of OH stretching of hydroxyl groups on EF species (3700-3650 $cm^{-1}$) is found also in the other spectra. In the case of H-BEA a weak band is observed at 3780 $cm^{-1}$, attributed too to EF OH groups. Thus the presence of EF species is evident for HY and H-BEA samples, but cannot be fully excluded in the other cases.

The spectra of alumina and silica alumina in the OH stretching region have been discussed previously [30]. What is relevant to remind here is that the IR spectrum of the silica alumina sample only shows a strong sharp band at ca. 3745 $cm^{-1}$, with a tail extending to lower frequencies. No bands are found in the region below 3700 $cm^{-1}$.

*3.1.2. IR study of CO adsorption.*

In Fig. 2, the spectra of CO adsorbed on H-USY zeolite is presented. The interaction of CO at 133 K gives rise to four different CO stretching bands (νCO) at 2229, 2180, 2156 and 2139 $cm^{-1}$. The band at 2229 $cm^{-1}$ is attributed due to CO interacting with strong Lewis sites, i.e. coordinatively unsaturated $Al^{3+}$ ions, whose Lewis acid strength is apparently similar to that of the strongest Lewis acid sites observed on silica alumina and alumina [30]. The band at 2180 $cm^{-1}$ is due to CO species interacting with the Brønsted acidic bridging hydroxyl groups, in this case the supercage OHs. CO interacting with terminal silanols gives rise to the band at 2156 $cm^{-1}$, while the band at 2139 $cm^{-1}$ is due to nearly liquid CO.

Looking at the spectra of OH stretching region in Fig. 2, it is evident that the HF band (3657 $cm^{-1}$, OHs located in the supercage) fully disappears, and shifts down to 3286 $cm^{-1}$ after interacting with CO, while the LF band (OHs located in the sodalite cages) is unperturbed, being these sites non accessible to CO. According to the so-called "hydrogen bonding method" [38] arising from the Bellamy-Hallam-Williams relation, the extent of shift down suffered by the νOH band, ΔνOH, can be taken as a measure of the strength of the H-bonding interaction, thus giving a measure of the Brønsted acid strength of the surface hydroxyl groups. The shifts down for the HF band of H-USY zeolite, ΔνOH = 347 $cm^{-1}$, indicates a very strong acidity of these groups. The sites responsible for the LF band, not accessible to CO are certainly not accessible also to ethanol, thus are likely not active in the reaction studied here.

For the materials under study, the shifting down of the OH groups after interaction with CO, obtained by similar experiments, are reported in Table 2. In case of H-FER, H-MOR and H-MFI samples, the measured ΔνOH value is also very high, but lower than for of H-USY. In case of H-Y, the position of perturbed band is at higher frequency than that of most zeolites, ΔνOH being lower than that of other zeolites. According to this method, zeolites have much stronger Brønsted acidity than alumina, in agreement also with the results of pyridine adsorption experiments [30], while silica alumina OHs should have intermediate Brønsted acidity except perhaps a small fraction of them that, although being terminal, would give rise to extensive shift down thus being almost as acidic as the bridging sites of most zeolites [31,38]. On the other hand, the CO stretching frequency of carbon monoxide adsorbed on OHs presents, on silica alumina, two components at 2173

and 2156 $cm^{-1}$, thus at lower frequency than that found on some zeolites and, in particular, H-USY (2180 $cm^{-1}$) which appears to be the strongest Brønsted acid. As for zeolites, these data would suggest that Brønsted acidity is quite similar among them, H-USY being perhaps the strongest Brønsted acid and H-Y being the weakest one, while all other would have similar Brønsted acidity. Actually, small differences in the $\Delta\nu$OH among zeolites may arise from additional Van Der Waals interactions as well as from different O-H-(CO) angles caused by the compression of the CO molecule on the opposite walls of the cavities. These effects are possible causes of discrepancy between $\Delta\nu$OHs and CO adsorption enthalpies reported previously [39]. However, we may mention that the multiplicity of OH groups with different behaviors and the additional roles of extraframework and external sites have also been totally neglected in ref. [39]. Additionally, as proposed by Chakarova and Hadjiivanov [40,41] the bands of OH groups interacting with CO can also perturbed by Fermi resonances in some zeolites. In any case, the small differences in the $\Delta\nu$OH among zeolites can be not entirely due to different Brønsted OH's acidities.

*3.1.3. Surface acidity characterization by IR spectroscopy of adsorption of pyridine.*

The spectra of pyridine adsorbed on silica alumina and alumina have been discussed previously [30]. Pyridine adsorbed on alumina gives rise to three 8a components observed at 1589-95, 1610-16 and 1624 $cm^{-1}$, revealing the existence of at least three different families of Lewis acid sites, and no significant Brønsted acidity. It seems likely [42,43] that the most acidic sites are predominantly located on corners and edges in the nanocrystals of aluminas. In the spectra of the silica alumina sample, the features of pyridine adsorbed on very strong Lewis sites is also evident (8a mode at 1623 $cm^{-1}$, 8b mode at 1579 $cm^{-1}$, 19b mode at 1454-6 $cm^{-1}$) together with the bands associated to pyridinium ions at 1633-31 $cm^{-1}$, 8a, and 1545 $cm^{-1}$, 19a [30]. This corresponds to the well-known Brønsted acidity of part of the hydroxyl groups of silica alumina, present together with very strong Lewis acid sites of the $Al^{3+}$ type.

The spectra of pyridine adsorbed on zeolites (Fig. 3) all present the features of pyridinium ions (in particular the 19a band at 1545 $cm^{-1}$), as the result of their Brønsted acidity. They also present, after outgassing at r.t., bands of molecular pyridine (in particular the 19b band at 1445-1440 $cm^{-1}$, together with 8a bands ion the 1600-1595 $cm^{-1}$ region), attributed to H-bonded pyridine. After outgassing at higher temperatures (523 K) the 19b band of

Lewis bonded pyridine is observed, relatively weak, at ca. 1455 $cm^{-1}$ in the case of H-FER and H-MOR but definitely intense, relative to the 19a mode of pyridinium ions, not only in the case of the H-Y sample (where a large amount of EF alumina certainly is present), but also in H-BEA and in H-USY. In contrast, this band is essentially not found on the two H-MFI samples, whose Al amount is low. It must be mentioned that, as discussed several years ago [44], the size of the cavities of FER zeolite does not allow the easy diffusion of pyridine at room temperature: thus the spectrum recorded on this sample in these conditions reflects the acidity of the external surface more than that of the internal one. Additionally, pyridine does not enter the "side pockets" of the MOR porous structure [45] as well as the sodalite cage and the hexagonal prisms of faujasites [36,34]. Also in the case of H-BEA, one of the two channels is expected to be diffused by pyridine with much difficulty, being its diameter too small [32]. The pyridine adsorption experiments confirm the presence of Brønsted sites in the case of all zeolites, but also shows in most cases Lewis sites having comparable strengths than those of alumina and silica alumina. Only the two H-MFI samples do not show significant amounts of pyridine bonded to Lewis acid sites. Thus, in these cases, that also do not show significant absorption in the region of the $\nu$OH of hydroxyl groups bonded to EF material, Al ions can be supposed to be essentially all in the framework positions. Thus for these materials it can be supposed that the number of Al ions corresponds to that of active protons. In the other cases the observation of Lewis sites suggests that part of Al ions may be extraframework, thus not corresponding to active protons.

*3.2. Catalytic conversion of ethanol.*

In Fig. 4 the effect of temperature on ethanol conversion over the zeolite catalysts is shown. Data concerning pure alumina and silica alumina [30] are also reported for comparison. Fig. 5 shows the selectivities (S) to C-containing products of ethanol over zeolite catalysts as a function of reaction temperature. These experiments have been performed using the same catalysts weight with the same feed conditions.

The catalytic activity on all zeolite samples starts to be significant at 373-393 K, while on silica alumina and alumina in the same conditions activity is observed at more than 400 K and 450 K, respectively. In all cases DEE is the main product. In parallel, conversion at moderate temperature such as 473 K is much higher on all zeolites (> 45 %) than on silica alumina and alumina (both < 20%). Also the H-MFI (280) sample, in spite of its very small

Al content, that results in a very low density of protonic sites, is definitely more active, at least in the 373-473 K range, than alumina and silica alumina. Thus it is evident that zeolites are definitely more active in converting ethanol than alumina and silica alumina (in terms of activity per weight). The apparent activation energies measured at low conversion are well above 80 kJ/mol in all cases, showing that diffusion limitation phenomena do not influence the activity in the low conversion range.

Among our zeolite samples an activity (per catalyst weight) trend H-MOR > H-MFI (50) > H-BEA ≈ H-FER > H-MFI (280) ≈ H-USY > H-Y is found, e.g. at 413 K. This trend is certainly influenced both by the different structures and by the different Al and proton contents of the samples. In Table 3 the ethanol conversion rates per Al ions are compared for zeolite samples at 413 K. At this temperature, conversion is in the range 1-17 % on all catalysts and it is determined by kinetics. The numbers we obtain here are closely similar to those reported by Chiang and Bhan who used the same FER and MOR samples [25] and referred the data to the proton content. Indeed, these values are equivalent to the conversion rates per proton only assuming that all Al ions are in the framework and generate an active proton each. This assumption, taken e.g. in ref. [25], is actually not valid in most cases, because part of Al ions are EF or located at the external surface, thus acting as Lewis acid sites, and also because part of hydroxyl groups may be unaccessible like in the case of faujasites. In fact, the greater ethanol conversion rates per Al ion are observed on H-MFI (280), and, to a lesser extent, on H-MFI (50), where the amount of Lewis acidity is very small or nothing, and EF species are essentially not observed. This is likely an evidence of the inactivity of part of protons, or of the location of part of Al ions out of the framework, in the more Al-charged samples. It is interesting that the conversion per Al site on H-MFI (280) is higher than on H-MFI (50), both catalysts supposed to be EF-free. It is possible to suppose that isolated protons are most active, possibly because several protons in the same channel can in some way hinder each other.

Over all catalysts, the selectivity to DEE is high at low temperature when also conversion is low or moderate (Fig. 5), while the selectivity to ethylene increases by rising temperature becoming almost total when conversion becomes very high. At low or moderate temperatures and conversions, the selectivity to ethylene is definitely higher on H-MOR than on other zeolites, at the same conversion / temperature, at the expense of selectivity to diethyl ether. In fact, only H-MOR and silica alumina give rise to significant selectivity to ethylene also at low temperature and conversion. This suggests that indeed H-MOR

structure in some ways favours ethylene production in conditions where DEE is the main product. Thus, the highest ethanol conversion on H-MOR is not really attributed to its Al content, relatively high, but at least in part to its structural features.

As a result, maximum yields to DEE are obtained on H-MFI (50) at 453-473 K and on H-BEA at 473 K (> 70 %) (Fig. 6), while almost total yield (> 99 %) to ethylene is obtained of H-FER at 523 K and more, and on faujasites, alumina and silica alumina at 573 K and more.

Additional products, such as hydrocarbons from $C_3$ to $C_5$ and $C_{6+}$ aromatics are obtained in significant amount at total ethanol conversion on H-BEA, H-MOR and particularly on H-MFI (50) (Fig. 5). Interestingly, at high temperature (> 523 K) H-MFI (50) shows a drop in ethylene selectivity and high selectivity to aromatics (toluene, xylene and high-carbon benzene-derived). Yields to ethylene drop from 92.1 % at 523 K to 10.2 % at 623 K on H-MFI (50), which nearly corresponds to the start of the reactivity denoted as "ethanol to hydrocarbons" mostly reported at higher temperatures [46,47,48,49]. Interestingly, both smaller and bigger pore size zeolites but also the low Al-content H-MFI (280) did not produce significant amounts of aromatics.

*3.3. Effect of space velocity over H-MFI (280) zeolite.*

As shown above, H-MFI (280) shows the highest reaction rates per Al ion for ethanol conversion and DEE synthesis. This is attributed to the fact that only this catalyst is actually a "single site" one. For this catalyst only, it can be supposed that essentially all Al ions are framework and give rise to an isolated "zeolitic" proton each. Thus over this catalyst the effect of space velocity (SV) on ethanol conversion rate has been investigated. The ethanol conversion rate definitely depends on contact time, i.e. the lower the space velocity, the greater the conversion, as expected indeed. On the other hand, the DEE selectivity clearly has a reverse trend (Fig. 7). At lower space velocities the DEE selectivity drops on favour of ethylene selectivity. This datum can be interpreted assuming that the selectivities indeed depend on conversion, DEE being favoured at low conversions, i.e. when ethanol concentration is still high. This approach agrees with the data reported by Chiang and Bhan [25], who showed that, at least on H-MOR, DEE formation rate increases with increasing ethanol pressure while ethylene production do the reverse, at least in a low pressure range. Alternatively, it may be assumed that at low space velocities

the primary product DEE can convert to ethylene and water as reported elsewhere [13,50,51]:

$(C_2H_5)_2O \rightarrow 2\ C_2H_4 + H_2O$ (3)

To look deeper at this we considered the selectivities at the same conversion, at different SV and temperature (Fig. 7, left). As for example, at conversions in the range 81-83 %, the selectivity to DEE drops from 43.6 % to 8.1 % when temperature is increased from 523 to 573 K in spite of the simultaneous strong increase in space velocity from 0.7 to 7.0 $h^{-1}$. This shows that reaction temperature has definitely a stronger effect, at high conversion levels, to favour ethylene selectivity, than conversion itself, i.e. ethanol partial pressure. This result also suggests reaction (3) is not the predominant one in forming ethylene.

In short, the best interpretation of the data is that the reaction forming ethylene is associated to higher temperature dependence (i.e. higher activation energies) and lower ethanol reaction order than the reaction producing DEE. This explains the different selectivities in different conditions.

*3.4. Catalyst stability study.*

A study on stability on time on stream has been performed on catalysts showing high yield to ethylene, in conditions allowing conversion approaching 100 %, until 405 min. The data are summarized in Table 4. H-USY and H-FER catalysts at 573 K show stable 99.9 % yield to ethylene with 0.1 % yield to propene. Alumina also shows stable activity at 623 K but the yield to ethylene 98.1-98.9 % is stably affected by coproduction of ethane and propene.

*3.5. Characterization of the exhausted catalysts.*

The catalysts discharged from the reactor after the tests performed with increasing reaction temperature (last step at 623 K) have been characterized by UV-Vis, TG-DTA and Raman spectroscopy. While all fresh zeolite catalysts are white, as expected, some of them darkened upon reaction (Fig. 8). In particular, the spent H-MOR catalyst is very dark blue, spent H-BEA is dark grey, spent H-MFI (50) is pale grey, while spent H-FER and H-FAU still remain almost white, just change a little bit to yellow.

3.5.1. UV-Vis spectroscopy.

UV-Vis spectra of spent catalysts are presented in Fig. 9. According to the previous visual inspection, the spectra of H-BEA and H-MOR show strong absorptions in the visible region, while other zeolites show weak absorption at the scale reported in the figure (Fig. 9 left). The spectrum of spent H-MOR shows mainly a broad absorption with the maximum in the red region, with a pronounced tail in the near IR region. The exact shape of the absorption is made difficult to be determined by the presence of a discontinuous raise in absorption observed at 800 nm almost in all spectra due to an instrumental artifact. In any case some sharper maxima are superimposed to the main broad absorption at 728, 979 and 1091 nm. In contrast, the spectrum of spent H-BEA shows a very strong maximum at 413 nm, in the violet region, with less pronounced components at 494 and 586 nm, and only an absorption tail in the red region. The spectrum observed on spent H-MFI (50) is very similar to that observed for spent H-BEA but much less intense. Also the spectra observed on H-FER, H-Y and H-USY are closely similar but far even less intense. A maximum near 256 nm is more evident in the spectra of H-BEA, H-MFI (50) and H-FER than on the others.

The spectra in the visible region are due to the $\pi \rightarrow \pi^*$ transitions of unsaturated organic species. In agreement with the visual inspection, the different spectra observed suggest that more carbonaceous species are formed on H-MOR and H-BEA, less on H-MFI (50) and even less on the other zeolites. The different spectra and color of spent H-MOR and H-BEA point also to a different chemical structure of the carbonaceous species formed on these catalysts. The spectrum observed on H-BEA (more intense but similar to that found on H-MFI (50)), with a main maximum a little above 400 nm and components at higher wavelength, is similar to that observed upon conversion of hydrocarbons and other organics on other zeolites [52,53]: it can be attributed to linear polyaromatic species such as e.g. tetracene and pentacene derivatives. The spectrum observed on H-MOR extends to higher wavelengths, thus being assigned to molecules having larger $\pi$ electron delocalization, but is even broader. It can be supposed to be due to a more complex distribution of molecules with even more aromatic rings. The band centered at 256 nm in the spectra of H-BEA, H-MFI (50) and H-FER can be due to conjugated dienic species, precursor of coke species [53].

3.5.2. Raman spectroscopy.

The spent catalysts have also been investigated by using Laser Raman spectroscopy. Only in the case of H-MOR a well-defined Raman spectrum has been obtained (Fig. 10). Several Raman peaks are observed at ca. 1608, 1550, 1390, 1305, 1170 $cm^{-1}$. The most intense peaks at 1608 and 1550 $cm^{-1}$ correspond to C=C stretching vibrations of $sp^2$ C=C bonds whether in chains or in aromatic rings [54,55]. The higher frequency peak is typically observed in the Raman spectra of coked zeolites and has been assigned to "disordered" polyaromatic coke structures, to which the peak at 1390 $cm^{-1}$ ("breathing" mode) can be associated [56,57]. The lower frequency component at 1550 $cm^{-1}$ is frequently present in graphite-like structures such as carbon nanotubes [58].

3.5.3. TG-DTA experiments

The combustion of carbon species formed on the most contaminated spent catalysts has been studied by TG-DTA. The TG weight loss and DTA curves of spent H-BEA, H-MOR and H-MFI (50) zeolites as a function of temperature are shown in Fig. 11. It is evident that the weight loss occurs at different temperatures for each catalyst, suggesting that there are different species of coke and/or various deposit locations. For H-BEA zeolite, the DTA curve indicates that a well-defined weight loss (ca 3 % wt/wt) observed starting at ca. 600 K and ending at 880 K, with corresponding an evident exothermic effect. The main heat evolution is centered at 800 K, with apparently another component around 700 K. In the case of H-MOR zeolite the main weight loss (> 7 % wt/wt) is observed at higher temperature (centered at ca. 860 K), confirming an higher amount of coke. For H-MFI (50) the weight loss is much lower (1 %) and, correspondingly, the DTA peak is also less evident, centred at ca. 800 K. The DTA peak at ca. 800-900 K can be assigned to the combustion of "hard" coke, essentially located in the zeolite cavities [59,60]. Maybe, the apparent splitting of the DTA peak in H-BEA is associated to the two different families of channels present in the structure.

## 4 Discussion

Looking at the overall conversion vs increasing temperature curves (Fig. 4), it is evident that zeolites are definitely more active in converting ethanol than alumina and silica alumina based on catalyst weight. Conversion of ethanol mainly to DEE starts at definitely lower temperature on zeolites, indicating that the different reactivity is not due to a difference in surface area but to a well different and more active reaction site. This is easily

understood in the case of the comparison of alumina and zeolites. It is very evident, and well-known indeed, that protonic zeolites display strong Brønsted acidity associated to the presence of the bridging hydroxyl groups responsible for the well-defined OH stretching band(s) in the region 3650-3550 $cm^{-1}$. These species are associated to the protonation of pyridine (Fig. 3) as well as to the strong interaction with CO giving rise to the shift down of the OH stretching band ($\Delta\nu \sim 300$ $cm^{-1}$, Table 2) and a CO stretching near 2180 $cm^{-1}$. Such a kind of Brønsted acidity is not present on alumina, that only presents Lewis acid sites, whose strength is, in any case, similar to that of Lewis sites found also in the case of all studied zeolites.

A more complex discussion is needed when the active sites of silica alumina are considered. Silica alumina, in fact, displays both strong Lewis acidity (pyridine bands at 1622, 1460 $cm^{-1}$, adsorbed CO absorbing at 2230 $cm^{-1}$) and significant Brønsted acidity (protonation of pyridine, strong adsorption of CO). However, silica aluminas usually do not present OH stretching bands at 3650-3550 $cm^{-1}$ associated to bridging OH's [29,30, 31,33]. This is in particular the case of our sample, which is a commercial cracking catalyst with typical characteristics, and can be taken as a reference material. This is particularly evident when considering the activity of the H-MFI (280) sample that, in spite of having a small Al content, has well evident the $\nu$OH band of the zeolitic hydroxyl groups at 3605 $cm^{-1}$ as well as significant activity at 393 K when silica alumina is still fully inactive. Thus the lower activity of silica alumina cannot be attributed to a lower number of zeolitic sites. As discussed previously [31,33], silica alumina OH's are essentially terminal although they may bridge upon interaction with basic molecules and they apparently have strong Brønsted acidity approaching those of protonic zeolites [61]. According to our previous conclusions [30], it seems likely that, for ethanol dehydration, silica alumina essentially works as a Lewis solid acid more than as a Brønsted solid acid. Thus, we attribute the catalytic activity of protonic zeolites to their Brønsted acid sites, that of silica alumina and alumina to their Lewis acid sites.

The comparison of the results concerning the catalytic activity and surface properties of the zeolite catalysts provide evidence of the following points:

1. The H-MOR sample is the most active catalyst in ethanol conversion. This result agrees with the data reported by Takahara et al. [13].

2. The H-MOR sample is also the only zeolite catalyst which shows some selectivity to ethylene also at low ethanol conversion. This also agrees with previous data [13,25].
3. Over all catalysts, at low temperature and conversion, DEE is produced with high selectivity, while at high temperature and conversion ethylene becomes the largely predominant product.
4. The selectivity to DEE is (at the same temperature and similar conversion level) higher for H-MFI and H-BEA than for other zeolites.
5. At high temperature almost total selectivity to ethylene is found on H-FER, H-Y and H-USY, while other products (higher hydrocarbons) are observed on H-BEA, H-MOR and, in particular, H-MFI (50), in agreement with the results of Stepanov et al. [62] and Wang et al. [23].
6. After the increasing reaction temperature experiments, coke is produced in significant amounts on H-MOR, less on H-BEA and much less in the other cases. Experimental data also indicate that carbon residues are larger in molecular size in H-MOR than in the other cases.
7. The Brønsted acid strength (as measured from IR spectroscopy of CO adsorption) seems to be similar for all zeolites, in agreement with Xu et al. [63], being possibly slightly stronger on H-USY and slightly weaker on H-Y than on the other zeolites.

The analysis of these data suggests that differences in Brønsted acid strengths do not play a main role in determining activities and selectivities in ethanol conversion over acid zeolite catalysts. The results are better interpreted assuming determinant roles of pore size and morphology (Fig. 12) through the two different effects, shape selectivity and confinement, as well as Al content.

As it is well known, shape selectivity is a key phenomenon making forbidden (or strongly inhibited) reactions involving transition states, intermediates and/or products whose size exceeds that of the catalyst cavities [64,65], thus somehow favouring competitive reactions. In contrast, confinement effect directly favour reactions whose transition states match the cavity size and are stabilized by the cavity [66].

The high ethanol conversion rates we measured for H-MOR can be attributed at least in part to the higher Al and proton content, ex. with respect to H-MFI samples, we found to be more active per Al ion. However, the higher ethylene vs DEE selectivity obtained on H-MOR than on all other solids at low temperature and conversion should be associated to

unique structural features of H-MOR. These peculiar structures are likely the so-called “side pockets” typical of this structure, where very likely one only molecule of ethanol can enter, favouring ethanol conversion and ethylene production, with respect to DEE production that obviously needs the reaction of two molecules. Thus sites located in the side pockets can be the most active and the most selective for unimolecular decomposition reaction of ethanol to ethylene. On larger cavities or open channels and low ethanol conversion this reaction suffers of the competition with the bimolecular reaction producing DEE.

On the other hand, medium pore zeolites such as H-MFI and H-BEA and, to a lesser extent, also H-MOR display the highest yields to DEE at moderate temperatures, as a combination of high ethanol conversion and high selectivity to the ether. It can be supposed that medium size channels are more favourable for this reaction than both larger cavities (such as those of faujasites) and smaller cavities such as those of ferrierite. On H-MFI (50) > 70 % yield to DEE is obtained at 453 K, with 72 % conversion and 98 % selectivity, ethylene being the only (useful) byproduct. This catalyst seems to be very effective for a heterogeneously catalysed ether synthesis process from (bio)ethanol.

The progressive decrease in DEE selectivity and increase in ethylene selectivity found at increasing temperature and conversion in all cases is explained by the different kinetic behaviour of the two reactions. Data obtained on H-MFI (280) support the idea that the change in selectivities is due to the higher activation energy and lower ethanol reaction order associated to ethylene production reaction with respect to DEE reaction.

Very high selectivity to ethylene and yield approaching 100 % have been obtained at high temperature and conversion on small pore H-FER and on large pore H-Y and H-USY. As discussed previously, over all catalysts when conversion becomes very high the DEE synthesis vanishes. The selectivity to ethylene in these high or total conversion conditions is limited by the production of higher olefins, paraffins and aromatics, occurring mostly in medium pore zeolites (H-MFI (50), H-MOR and H-BEA). This is particularly the case of H-MFI (50) which is in fact well-known to be particularly active in producing aromatics from several hydrocarbon sources such as butenes [67], paraffins [68], as well as vegetable oils [57,69,70]. Medium pore zeolites are also those producing more coke.

The high selectivity to ethylene at high conversion on H-FER can be explained by a product shape selectivity effect, being aromatics formation and diffusion in its channels substantially forbidden for steric reasons. The small size of the ferrierite channels can be

associated also to the limited formation of oligomers of ethylene, possibly associated to a transition state shape selectivity effect.

On the other hand, the increased formation of higher hydrocarbons, aromatics and coke on medium pore zeolites than on large pore zeolite can be associated to a confinement effect favouring polymerizations and cyclization/aromatization, due to an optimal size of the channels for transition states involved in these reactions. The optimal effect for producing single oligomeric and aromatic molecules is obtained in H-MFI (50) zeolite, while the larger channels of H-BEA and, even more, of H-MOR could be more effective for coking. This effect almost does not exist on H-MFI (280), which material also possesses MFI framework: this suggests that several Brønsted acid sites in the same channels are also needed for producing this reactivity, “isolated” sites, like those of H-MFI (280), being not active for this reaction. In addition, this confinement effect should relax in faujasites whose supercages are far larger.

## 5 Conclusions.

The main results of this research are the following:

1. Protonic zeolites are definitely more active than silica alumina and alumina in converting ethanol to DEE and ethylene. This is due to the presence of Brønsted acidic bridging hydroxyl groups only in the zeolite cavities. Silica alumina and alumina, that do not present these sites, are supposed to work as Lewis acid sites in this reaction.
2. H-MOR is the only zeolite catalyst (among those investigated here) which shows some selectivity to ethylene also at low ethanol conversion.
3. Over all catalysts, at low temperature and conversion diethyl ether is produced with high selectivity. On H-BEA and H-MFI (50) > 70 % yield to the ether is obtained at 453-473 K.
4. Over all these catalysts, at high temperature and conversion ethylene becomes the largely predominant product. This is likely due to higher activation energies and lower ethanol reaction order of the reaction forming ethylene with respect to the reaction forming diethyl ether.
5. Over both H-FER and H-USY stable 99.9 % yield to ethylene is obtained at 573 K with no deactivation at least for 405 min. These zeolites outperform alumina at least until this time on stream.

6. Over H-MFI (50) at full conversion selectivity to ethylene drops while a number of higher hydrocarbons and high yields to aromatics (~ 29 %) are obtained. This is not found on the low Al content zeolite H-MFI (280).
7. H-MOR and, to a lesser extent, H-BEA suffer coking much more than all other catalysts.
8. This behaviour provides evidence of a main role of confinement effects and, secondarily, of shape selectivity and number of acid sites, more than of strength of acid sites of zeolites for these reactions.

**Acknowledgements**

The collaboration of M.M. Carnasciali and G. Garbarino for recording Raman spectra is acknowledged. TKP acknowledges funding by EMMA in the framework of the EU Erasmus Mundus Action 2. The authors acknowledge University of Genova for partial funding (PRA2013).

**Table 1. The properties of investigated catalysts**

| Notation | Commercial name | Manufacturer | Preparation | $SiO_2/Al_2O_3$ mol ratio | $S_{BET}$[a] | Na (%)[b] |
|---|---|---|---|---|---|---|
| AL | Puralox Sba200 | Sasol | as received | - | ~ 190 | 0.002 |
| SA | Silica alumina (13%wt $Al_2O_3$) | Strem Chemicals | as received | 11.4 | ~ 330 | - |
| H-FER | CP 914C | Zeolyst | Calcined at 773 K, 4h | 20 | ~ 400 | 0.05 |
| H-MFI (280) | CBV 28014 | Zeolyst | Calcined at 773 K, 4h | 280 | ~ 400 | 0.05 |
| H-MFI (50) | CBV 5524G | Zeolyst | Calcined at 773 K, 4h | 50 | ~ 425 | 0.05 |
| H-MOR | CBV 21A | Zeolyst | Calcined at 773 K, 4h | 20 | ~ 500 | 0.08 |
| H-BEA | CP 814E | Zeolyst | Calcined at 773 K, 4h | 25 | ~ 680 | 0.05 |
| H-Y | CBV 400 | Zeolyst | as received | 5.1 | ~ 730 | 2.8 |
| H-USY | CBV 720 | Zeolyst | as received | 30 | ~ 780 | 0.03 |

[a, b] from manufacturer

**Table 2. Position of OH stretching band of zeolite before and after CO adsorption**

| Samples | before CO adsorption | after CO adsorption | $\Delta\nu OH$ | $\nu CO$ (H-bond) |
|---|---|---|---|---|
| AL | 3790, 3770, 3725 | 3610 | 180-110 | 2156 |
| SA | 3747-3740 | 3667, 3580 (3415) | 80, 167 (320) | 2173,2156 |
| H-FER | 3635 | 3316 | 319 | 2171 |
| H-MFI (50) | 3610 | 3294 | 316 | 2174 |
| H-MOR | 3612 | 3293 | 319 | 2174 |
| H-BEA | 3605 | 3300 | 305 | 2178 |
| H-Y | 3620 | 3325 | 295 | 2165 |
| H-USY | 3633 | 3286 | 347 | 2180 |

**Table 3. Rate of ethanol conversion per Al ion ($10^5$ mol EtOH reacted (mol Al)$^{-1}$ s$^{-1}$) at 413 K.**

| H-FER | H-MFI (280) | H-MFI (50) | H-MOR | H-BEA | H-Y | H-USY |
|---|---|---|---|---|---|---|
| 39.9 | 336.1 | 155.0 | 93.0 | 53.9 | 2.2 | 20.7 |

**Table 4. Conversion and selectivities to C-containing products of ethanol over alumina and zeolites as a function of time on stream.**

| Catalyst | Time (min.) | Total conversion | S diethyl ether | S ethylene | S ethane | S propene |
|---|---|---|---|---|---|---|
| **AL 623 K** | 45 | 100.0 | 0.0 | 98.9 | 1.0 | 0.1 |
| | 90 | 100.0 | 0.0 | 98.8 | 1.2 | 0.1 |
| | 135 | 100.0 | 0.0 | 98.8 | 1.2 | 0.1 |
| | 180 | 100.0 | 0.0 | 98.7 | 1.3 | 0.1 |
| | 225 | 100.0 | 0.0 | 98.5 | 1.4 | 0.1 |
| | 270 | 100.0 | 0.0 | 98.1 | 1.8 | 0.1 |
| | 315 | 100.0 | 0.0 | 98.7 | 1.3 | 0.0 |
| | 360 | 100.0 | 0.0 | 98.5 | 1.4 | 0.1 |
| | 405 | 100.0 | 0.0 | 98.5 | 1.4 | 0.0 |
| **H-FER 573 K** | 45 | 100.0 | 0.0 | 99.9 | 0.0 | 0.1 |
| | 90 | 100.0 | 0.0 | 99.9 | 0.0 | 0.1 |
| | 135 | 100.0 | 0.0 | 99.9 | 0.0 | 0.1 |
| | 180 | 100.0 | 0.0 | 99.9 | 0.0 | 0.1 |
| | 225 | 100.0 | 0.0 | 99.9 | 0.0 | 0.1 |
| | 270 | 100.0 | 0.0 | 99.9 | 0.0 | 0.1 |
| | 315 | 100.0 | 0.0 | 99.9 | 0.0 | 0.1 |
| | 360 | 100.0 | 0.0 | 99.9 | 0.0 | 0.1 |
| | 405 | 100.0 | 0.0 | 99.9 | 0.0 | 0.1 |
| **H-USY 573 K** | 45 | 100.0 | 0.0 | 99.9 | 0.0 | 0.1 |
| | 90 | 100.0 | 0.0 | 100.0 | 0.0 | 0.0 |
| | 135 | 100.0 | 0.0 | 99.9 | 0.0 | 0.1 |
| | 180 | 100.0 | 0.0 | 99.9 | 0.0 | 0.1 |
| | 225 | 100.0 | 0.0 | 99.9 | 0.0 | 0.1 |
| | 270 | 100.0 | 0.0 | 99.9 | 0.0 | 0.1 |
| | 315 | 100.0 | 0.0 | 99.9 | 0.0 | 0.1 |
| | 360 | 100.0 | 0.0 | 99.9 | 0.0 | 0.1 |
| | 405 | 100.0 | 0.0 | 99.9 | 0.0 | 0.1 |

**Figure Captions**

Fig. 1. FT-IR spectra of pure zeolites after activation at 773 K (νOH region)

Fig. 2. FT-IR spectra of surface species (νOH region) arising from CO adsorption on H-USY zeolite. The insert: FT-IR spectra of surface species (νCO region) in the same experiment.

Fig. 3. FT-IR subtraction spectra of surface species arising from pyridine adsorbed on pure zeolites: (a) at room temperature and (b) outgassing at 523 K.

Fig. 4. Conversion of ethanol (96%) at atmospheric pressure in a fixed-bed tubular quartz reactor using 0.5 g of catalysts with 1.43 $h^{-1}$ WHSV in nitrogen from 373 K to 623 K.

Fig. 5. Conversion and selectivities to C-containing products of ethanol over zeolites as a function of reaction temperature (predominant compounds of others are benzene, toluene, xylenes, trimethylbenzenes and other mononuclear aromatics).

Fig. 6. Diethyl ether yield as a function of temperature. Reaction condition: at atmospheric pressure in a fixed-bed tubular quartz reactor using 0.5 g of catalysts with 1.43 $h^{-1}$ WHSV in nitrogen from 373 K to 623 K.

Fig. 7. Conversion and selectivities to C-containing products of ethanol over H-MFI (280) at different space velocities (left); Conversion, diethylether selectivity and ethylene selectivities on H-MFI (280) at 523 K as a function of space velocity (right).

Fig. 8. The photograph of spent zeolites after reaction with increasing temperature from 373 K to 623 K.

Fig. 9. UV-Vis spectra of spent zeolites after reaction with increasing temperature from 373 K to 623 K.

Fig. 10. Raman spectra of spent H-MOR zeolite after reaction with increasing temperature from 373 K to 623 K, that was performed in continuous condition: 4000-100 $cm^{-1}$, 1 accumulation and 1% laser power of He-Ne laser at 632.8 nm.

Fig. 11. TG-DTA curves of spent H-BEA, H-MOR and H-MFI after reaction with increasing temperature from 373 K to 623 K, under air flow.

Fig. 12. Schematics of the cavities in zeolite structures (IZA database).

**References**


[1] W.R. True, Oil and Gas Journal, http://www.ogj.com/articles/print/volume-111/issue-7/special-report-ethylene-report/global-ethylene-capacity-poised-for-major.html

[2] OECD SIDS Initial assessment Profile-Ethylene; INCHIM, 2008 http://www.inchem.org/documents/sids/sids/74851.pdf

[3] R.A. Meyers (ed.), Handbook of Petrochemicals Production Processes, Mc Graw Hill, 2005, part 6, pp. 6.1-6.63.

[4] The Ethylene Product Stewardship Manual, American Chemistry Council, 2004

http://www.lyondellbasell.com/techlit/techlit/Handbooks%20and%20Manuals/ACC_Ethylene_Manual%203096.pdf

[5] Q. Wu, W. Xia, A. Takahashi, T. Fujitani, Adv. Mat. Res. 538-541 (2012) 2417-2420.

[6] Y.C. Hu, in: J.J. McKetta (Ed.), Chemical Processing Handbook, Dekker, New York, 1993, p. 768.

[7] Ethylene from Ethanol, Chematur Engineering Group http://www.chematur.se/sok/download/Ethylene_rev_0904.pdf (20.05.2013)

[8] M. Caillot, A. Chaumonnot, M. Digne, J.A. van Bokhoven, J. Catal. 316 (2014) 47-56.

[9] R. Le Van Mao, T.M. Nguyen, G.P. McLaughlin, Appl. Catal. 48 (1989) 265-277.

[10] J.C. Oudejans, P.F. Van den Oosterkamp, H. Van Bekkum, Appl. Catal. 3 (1982) 109-115.

[11] C. de las Pozas, R. Lopez-Cordero, J.A. Gonzalez-Morales, N. Travieso, R. Roque-Malherbe, J. Mol. Catal. 83 (1993) 145-156.

[12] C.B. Phillips, R. Datta, Ind. Eng. Chem. Res. 36 (1997) 4466-4475.

[13] I. Takahara, M. Saito, M. Inaba, K. Murata, Catal. Lett. 105 (2005) 249-252.

[14] I. Takahara, M. Saito, H. Matsuhashi, M. Inaba, K. Murata, Catal. Lett. 113 (2007) 82-85.

[15] X. Zhang, R. Wang, X. Yang, F. Zhang, Micropor. Mesopor. Mater. 116 (2008) 210-215.

[16] K. Ramesh, L.M. Hui, Y.-F. Han, A. Borgna, Catal. Commun. 10 (2009) 567-571.

[17] J. Ouyang, F. Kong, G. Su, Y. Hu, Q. Song, Catal. Lett. 132 (2009) 64-74.

[18] M. Zhang and Y. Yu, Ind. Eng. Chem. Res. 52 (2013) 9505-9514.

[19] D. Fan, D.-J. Dai, H.-S. Wu, Mater. 6 (2013) 101-115.

[20] A. Zecchina, S. Bordiga, G. Spoto, D. Scarano, G. Spano, F. Geobaldo, J. Chem. Soc. Faraday Trans. 92 (1996) 4863-1875.

[21] C.-C. Lee, R.J. Gorte, W.E. Farneth, J. Phys. Chem. B 101 (1997) 3811-3817.

[22] J.N. Kondo, K. Ito, E. Yoda, F. Wakabayashi, K. Domen, J. Phys. Chem. B 109 (2005) 10969-10972.

[23] W. Wang, J. Jiao, Y. Jiang, S.S. Ray, M. Hunger, Chem. Phys. Chem. 6 (2005) 1467-1469.

[24] C.M. Nguyen, M.-F. Reyniers, G.B. Marin, Phys. Chem. Chem. Phys. 2 (2010) 9481-9493.

[25] H. Chiang, A. Bhan, J. Catal. 271 (2010) 251-261.

[26] J.H. Kwak, D. Mei, C.H.F. Peden, R. Rousseau, J. Szanyi, Catal. Lett. 141 (2011) 649-655.

[27] S. Roy, G. Mpourmpakis, D.-Y Hong, D.G. Vlachos, A. Bhan, R.J. Gorte, ACS Catal. 2 (2012) 1846-1853.

[28] J.F. DeWilde, H. Chiang, D.A. Hickman, C.R. Ho, A. Bhan, ACS Catal. 3 (2013) 798-807.

[29] M. Caillot, A. Chaumonnot, M. Digne, J.A. Van Bokhoven, Chem. Cat. Chem. 6 (2014) 832-841.

[30] T.K. Phung, A. Lagazzo, M.Á. Rivero Crespo, V. Sanchez Escribano, G. Busca, J. Catal. 311 (2014) 102-113.

[31] M. Bevilacqua, T. Montanari, E. Finocchio, G. Busca, Catal. Today 116 (2006) 132-142.

[32] T. Montanari, M. Bevilacqua, G. Busca, Appl. Catal. A 307 (2006) 21-29.

[33] G. Busca, Chem. Rev. 107 (2007) 5366-5410.

[34] T. Montanari, E. Finocchio, G. Busca, J. Phys. Chem. C 115 (2011) 937-943.

[35] T.K. Phung, M.M. Carnasciali, E. Finocchio, G. Busca, Appl. Catal. A 470 (2014) 72-80.

[36] W. Daniell, N.-Y. Topsøe, H. Knözinger, Langmuir 17 (2001) 6233-6239.

[37] H.S. Cerqueira, P. Ayrault, J. Datka, M. Guisnet, Micropor. Mesopor. Mater. 38 (2000) 197-205.

[38] G. Busca, Catal. Today 41 (1998) 191-206.

[39] C. Otero Arean, M. R. Delgado, P.Nachtigall, Ho Viet Thang, M.Rubes, R. Bulanek, P. Chlubna-Eliasova, Phys. Chem. Chem. Phys., 16 (2014) 10129-10141.

[40] K. Chakarova, K. Hadjiivanov, Chem. Commun. 47 (2011) 1878–1880

[41] K. Chakarova, K. Hadjiivanov, Micropor. Mesopor. Mater. 177 (2013) 59–65.

[42] G. Busca, Catal. Today 226 (2014) 2-13.

[43] T.K. Phung, C. Herrera, M. Ángeles Larrubia, M. García-Diéguez, E. Finocchio, L.J. Alemany, G. Busca, Appl. Catal. A 483 (2014) 41-51.

[44] M. Trombetta and G. Busca, J. Catal. 187 (1999) 521-523.

[45] M. Bevilacqua, A. Gutièrrez Alejandre, C. Resini, M. Casagrande, J. Ramirez and G. Busca, Phys. Chem. Chem. Phys. 4 (2002) 4575-4583.

[46] Y.I. Makarfi, M.S. Yakimova, A.S. Lermontov, V.I. Erofeev, L.M. Koval, V.F. Tretiyakov, Chem. Eng. J. 154 (2009) 396-400.

[47] M. Inaba, K. Murata, M. Saito, I. Takahara, React. Kinet. Catal. Lett. 88(1) (2006) 135-141.

[48] K. Inoue, M. Inaba, I. Takahara, K. Murata, Catal. Lett. 136 (2010) 14-19.

[49] A.T. Aguayo, A.G. Gayubo, A.M. Tarrío, A. Atutxa, J. Bilbao, J. Chem. Technol. Biotechnol. 77 (2002) 211-216.

[50] K. Yasunaga, F. Gillespie, J.M. Simmie, H.J. Curran, Y. Kuraguchi, H. Hoshikawa, M. Yamane, Y. Hidaka, J. Phys. Chem. A 114 (2010) 9098–9109.

[51] M.A. Christiansen, G. Mpourmpakis, D.G. Vlachos, ACS Catal. 3 (2013) 1965-1975.

[52] L.M. Petkovic, D.M. Ginosar, K.C. Burch, J. Catal. 234 (2005) 328-339.

[53] M.J. Wulfers, F.C. Jentoft, J. Catal. 307 (2013) 204-213.

[54] B. Guichard, M. Roy-Auberger, E. Denvers, B. Rebours, A.A. Quoineaud, M. Digne, Appl. Catal. A 367 (2009) 1-8.

[55] J. Li, G. Xiong, Z. Feng, Z. Liu, Q. Xin, C. Li, Micropor. Mesopor. Mater. 39 (2000) 275-280.

[56] P. Castaño, G. Elordi, M. Olazar, A.T. Aguayo, B. Pawelec, J. Bilbao, Appl. Catal. B 104 (2011) 91-100.

[57] J.A. Botas, D.P. Serrano, A. García, J. De Vicente, R. Ramos, Catal. Today 195 (2012) 59-70.

[58] A.M. Rao, S. Bandow, , E. Richter, P.C. Eklund, Thin Solid Films 331 (1998) 141-147.

[59] A.R. Pradhan, J.F. Wu, S.J. Jong, T.C. Tsai, S.B. Liu, Appl. Catal. A 165 (1997) 489-497.

[60] H.S. Cerqueira, G. Caeiro, L. Costa, F. Ramoa Ribeiro, J. Mol. Catal. A Chem. 292 (2008) 1-13.

[61] F. Leydier, C. Chizallet, A. Chaumonnot, M. Digne, E. Soyer, A.-A. Quoineaud, D. Costa, P. Raybaud, J. Catal., 284 (2011) 215-229.

[62] A.G. Stepanov, M.V. Luzgin, V.N. Romannikov, V.N. Sidelnikov, E.A. Paukshtis, J. Catal. 178 (1998) 466-477.

[63] B. Xu, C. Sievers, S.B. Hong, R. Prins, J.A. van Bokhoven, J. Catal. 244 ( 2006) 163-168.

[64] P.B. Weisz V.J. Frilette, J. Phys. Chem. 64 (1960) 382-382.

[65] B. Smit, T.L.M. Maesen, Nature 451 (2008) 671-678.

[66] R. Gounder, E. Iglesia, Acc. Chem. Res. 45 (2012) 229-238.

[67] M. Trombetta, G. Busca, S. Rossini, V. Piccoli, U. Cornaro, A. Guercio, R. Catani, R. J. Willey, J. Catal. 179 (1998) 581-596.

[68] A. Bhan, W.N. Delgass, Catal. Rev. – Sci. Eng. 50 (2008) 19-151.
[69] T.-A. Ngo, J.S. Kim, S.K. Kim, S.-S. Kim, Energy 35 (2010) 2723-2728.
[70] J.A. Botas, D.P. Serrano, A. García, R. Ramos, Appl. Catal. B 145 (2014) 205-215.

Figure 1

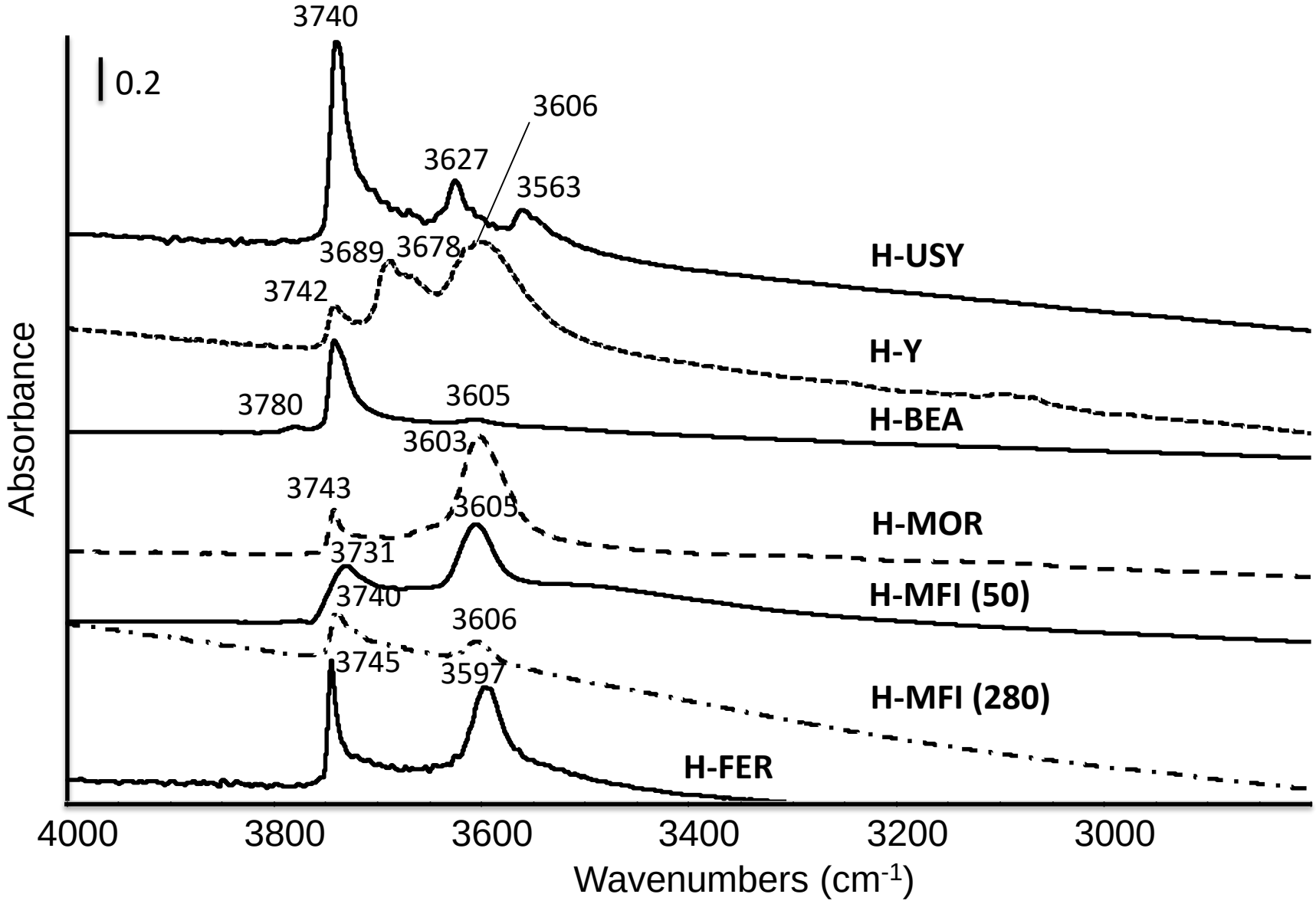
3740
0.2
3606
3627
3563
3689
3678
3742
H-USY
H-Y
3780
3605
H-BEA
3603
3743
3605
H-MOR
3731
3740
H-MFI (50)
3606
3745
3597
H-MFI (280)
H-FER
Absorbance
4000
3800
3600
3400
3200
3000
Wavenumbers (cm-1)

Figure 2

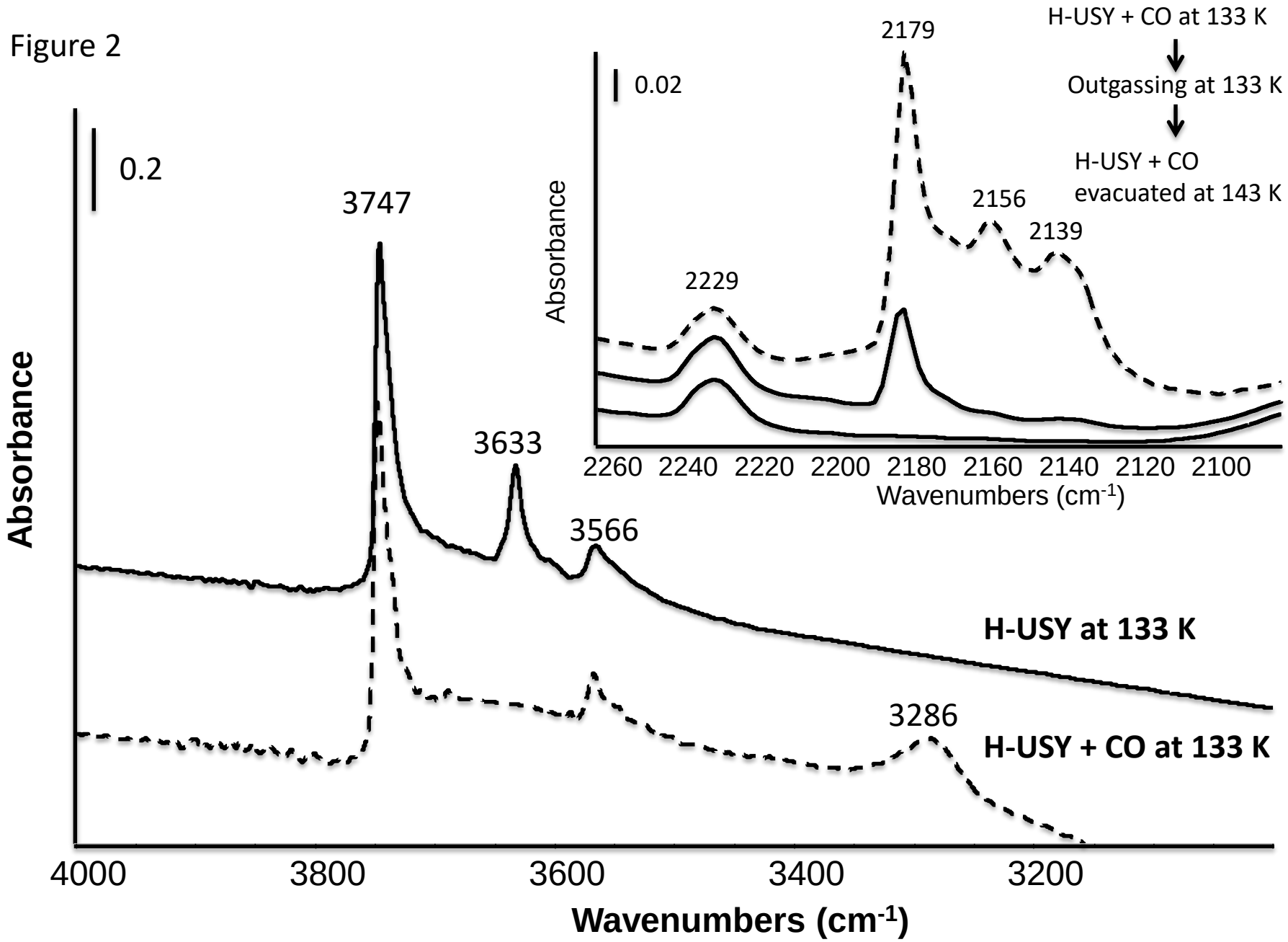
0.2
3747
3633
3566
3286
H-USY at 133 K
H-USY + CO at 133 K
Absorbance
4000
3800
3600
3400
3200
Wavenumbers (cm-1)
0.02
2179
2229
2156
2139
H-USY + CO at 133 K
Outgassing at 133 K
H-USY + CO
evacuated at 143 K
Absorbance
2260 2240 2220 2200 2180 2160 2140 2120 2100
Wavenumbers (cm-1)

Figure 3

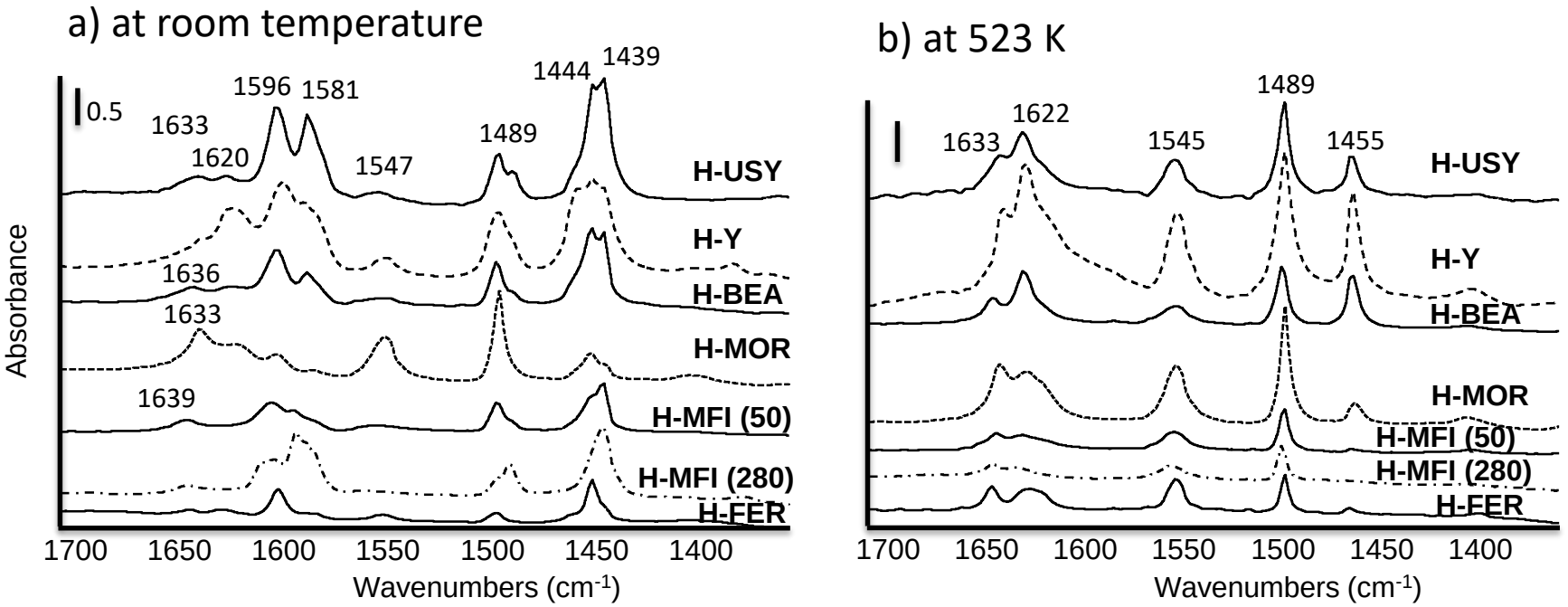
a) at room temperature
0.5
1633
1620
1596
1581
1547
1489
1444
1439
1636
1633
1639
H-USY
H-Y
H-BEA
H-MOR
H-MFI (50)
H-MFI (280)
H-FER
Absorbance
1700 1650 1600 1550 1500 1450 1400
Wavenumbers (cm-1)
b) at 523 K
1633
1622
1545
1489
1455
H-USY
H-Y
H-BEA
H-MOR
H-MFI (50)
H-MFI (280)
H-FER
1700 1650 1600 1550 1500 1450 1400
Wavenumbers (cm-1)

Figure 4

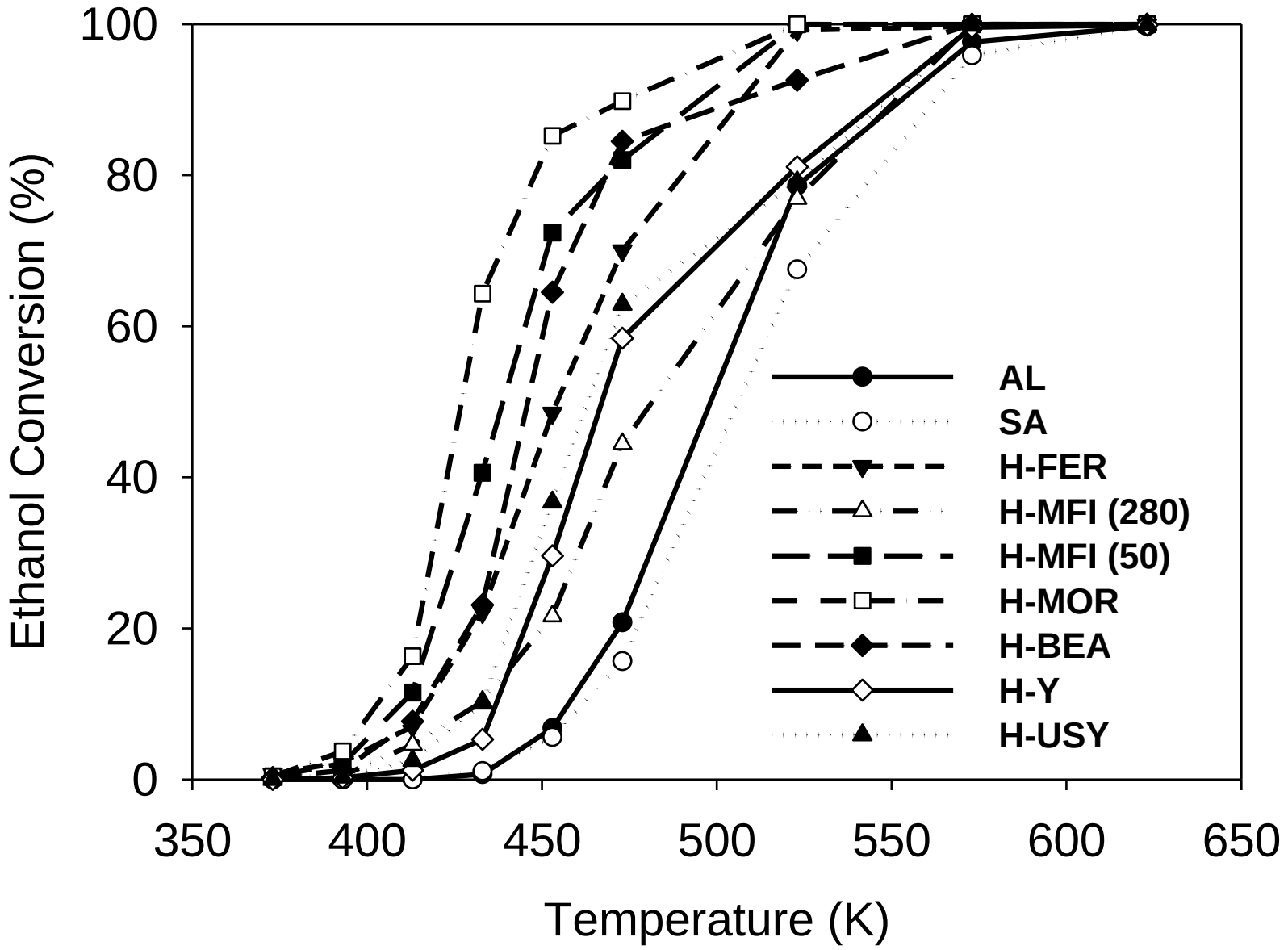
Ethanol Conversion (%)
100
80
60
40
20
0
350
400
450
500
550
600
650
Temperature (K)
AL
SA
H-FER
H-MFI (280)
H-MFI (50)
H-MOR
H-BEA
H-Y
H-USY

Figure 5

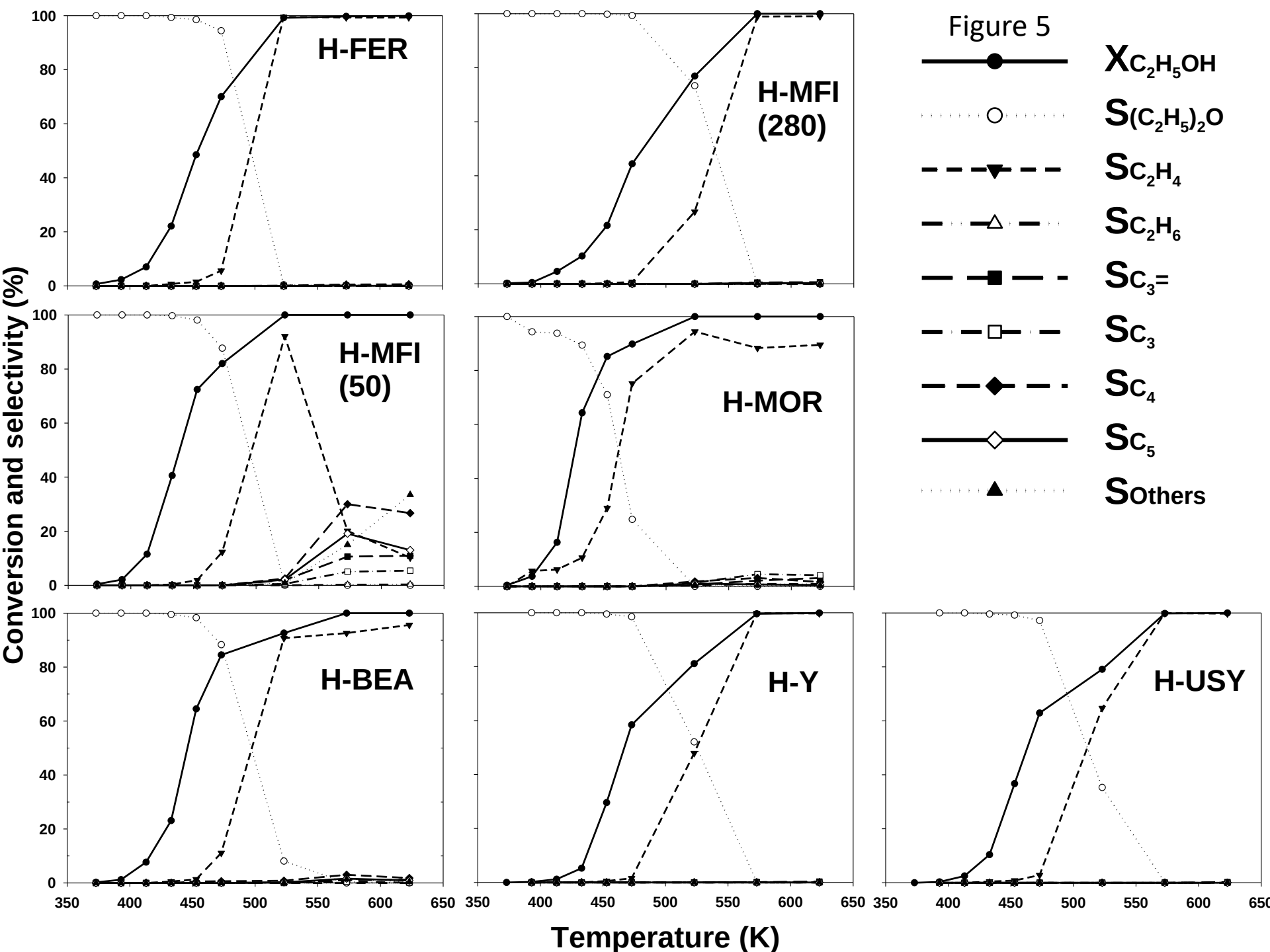
H-FER
H-MFI (280)
H-MFI (50)
H-MOR
H-BEA
H-Y
H-USY
Conversion and selectivity (%)
Temperature (K)
0
20
40
60
80
100
350
400
450
500
550
600
650
$X_{C_2H_5OH}$
$S_{(C_2H_5)_2O}$
$S_{C_2H_4}$
$S_{C_2H_6}$
$S_{C_3=}$
$S_{C_3}$
$S_{C_4}$
$S_{C_5}$
$S_{Others}$

Figure 6

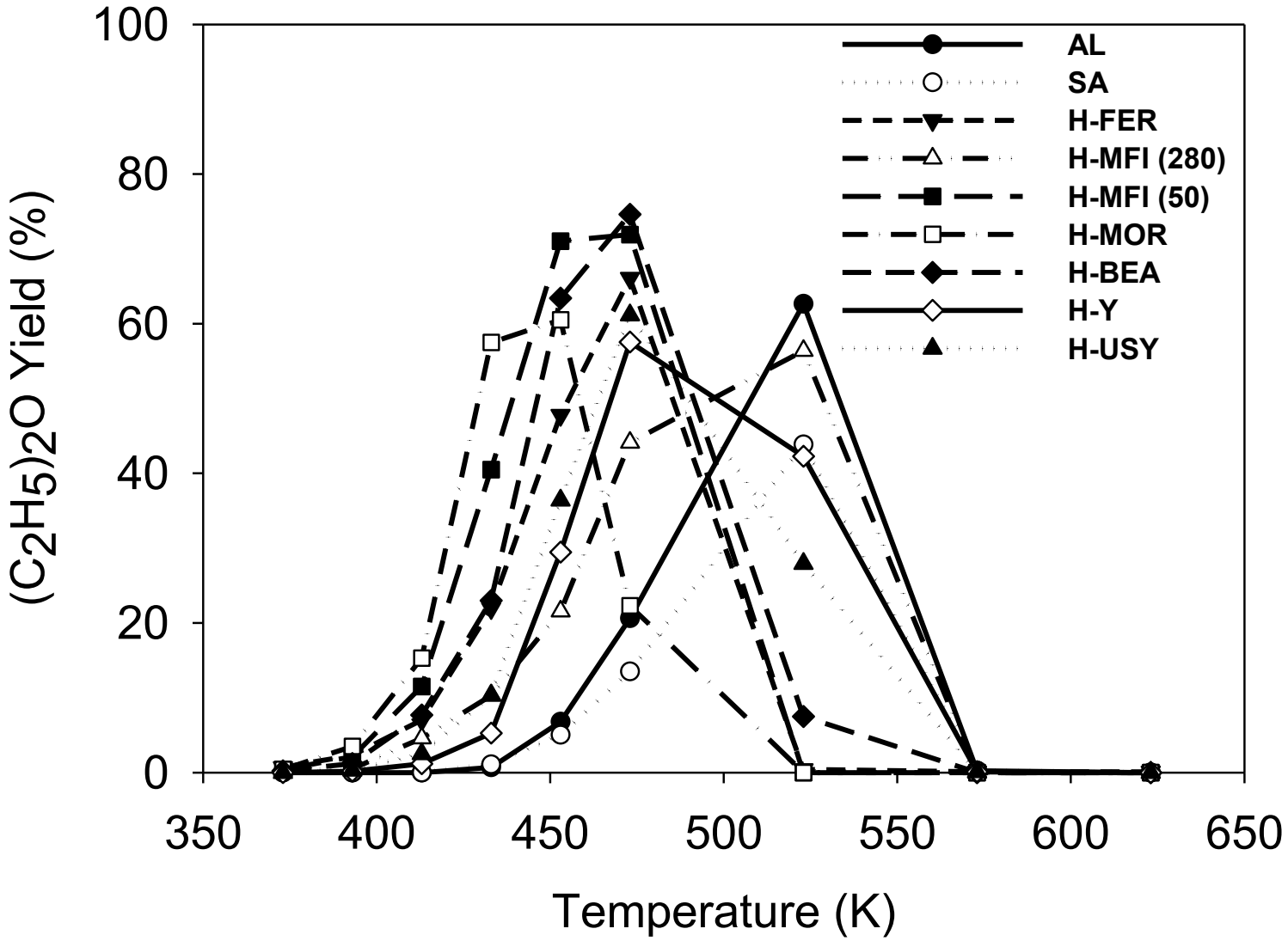
100
80
60
40
20
0
350
400
450
500
550
600
650
(C2H5)2O Yield (%)
Temperature (K)
AL
SA
H-FER
H-MFI (280)
H-MFI (50)
H-MOR
H-BEA
H-Y
H-USY

Figure 7

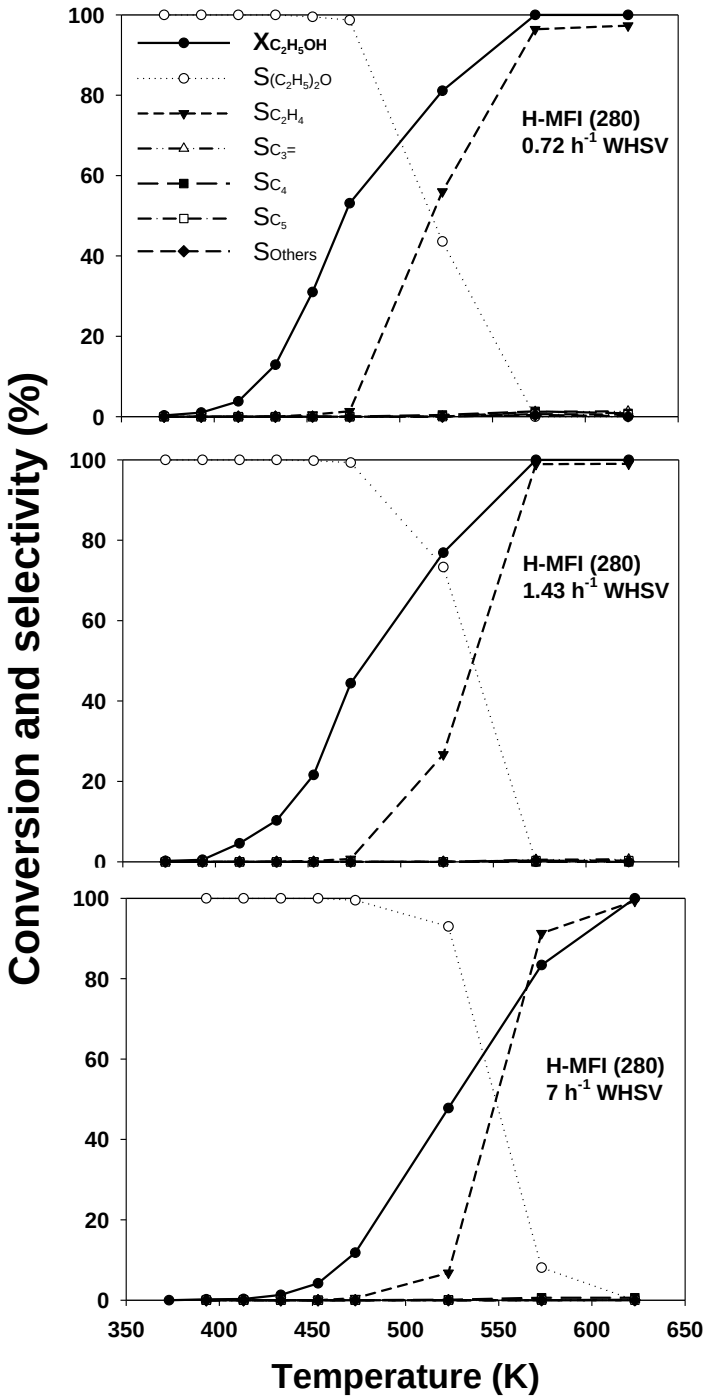
Conversion and selectivity (%)
$X_{C_2H_5OH}$
$S_{(C_2H_5)_2O}$
$S_{C_2H_4}$
$S_{C_3=}$
$S_{C_4}$
$S_{C_5}$
$S_{Others}$
H-MFI (280)
0.72 h-1 WHSV
H-MFI (280)
1.43 h-1 WHSV
H-MFI (280)
7 h-1 WHSV
Temperature (K)

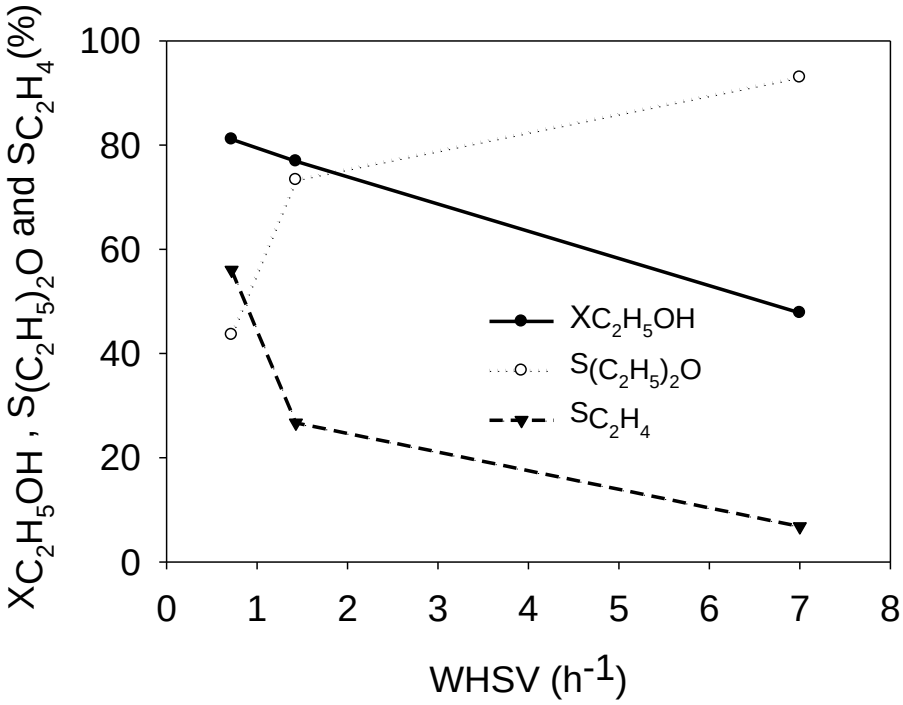
$XC_2H_5OH$ , $S(C_2H_5)_2O$ and $SC_2H_4$ (%)
$XC_2H_5OH$
$S(C_2H_5)_2O$
$SC_2H_4$
WHSV (h-1)

Figure 8

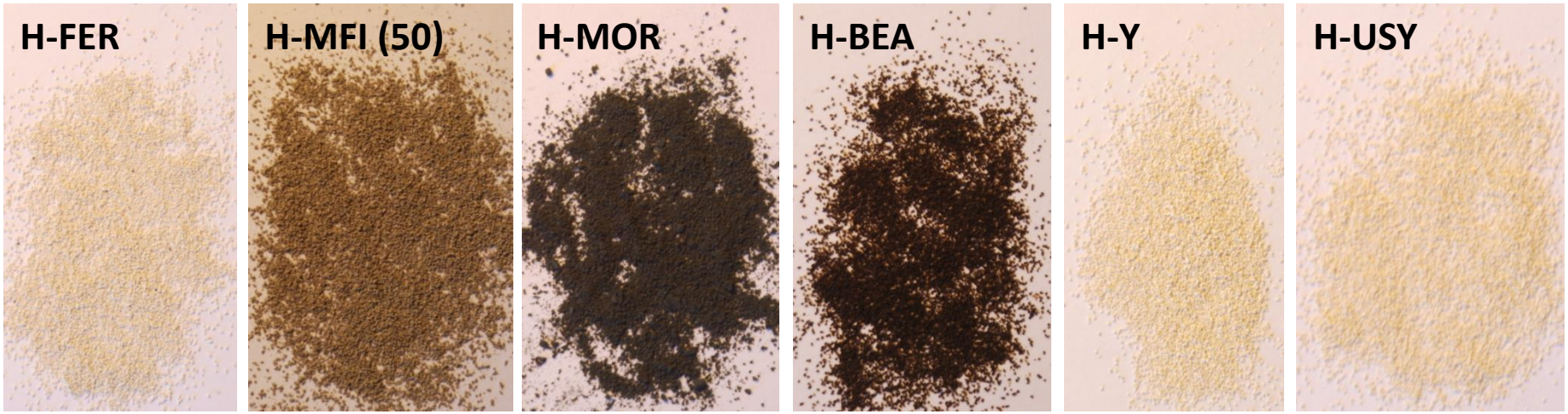

Figure 9

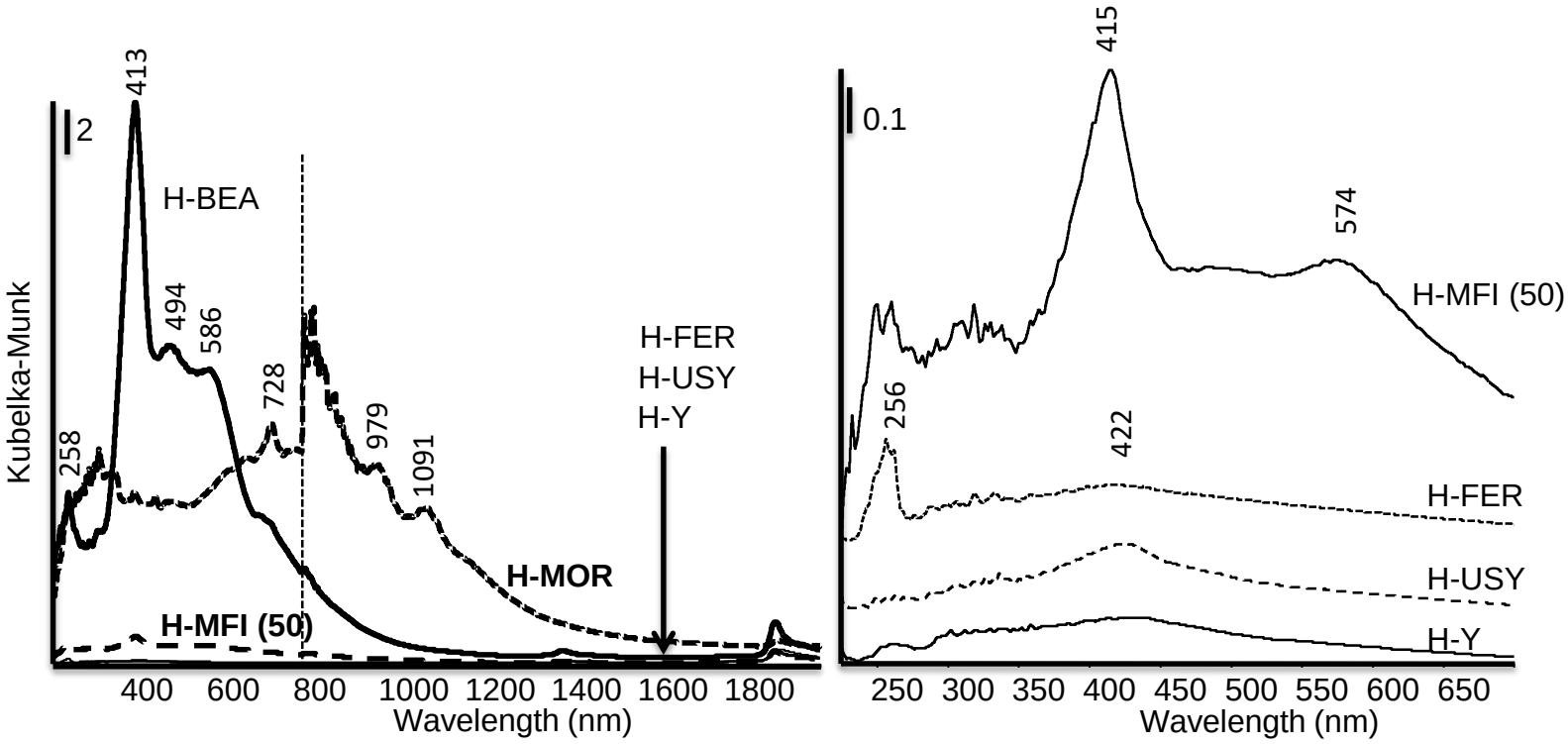
Kubelka-Munk
2
413
H-BEA
494
586
728
258
979
1091
H-FER
H-USY
H-Y
H-MOR
H-MFI (50)
400 600 800 1000 1200 1400 1600 1800
Wavelength (nm)
0.1
415
574
H-MFI (50)
256
422
H-FER
H-USY
H-Y
250 300 350 400 450 500 550 600 650
Wavelength (nm)

Figure 10

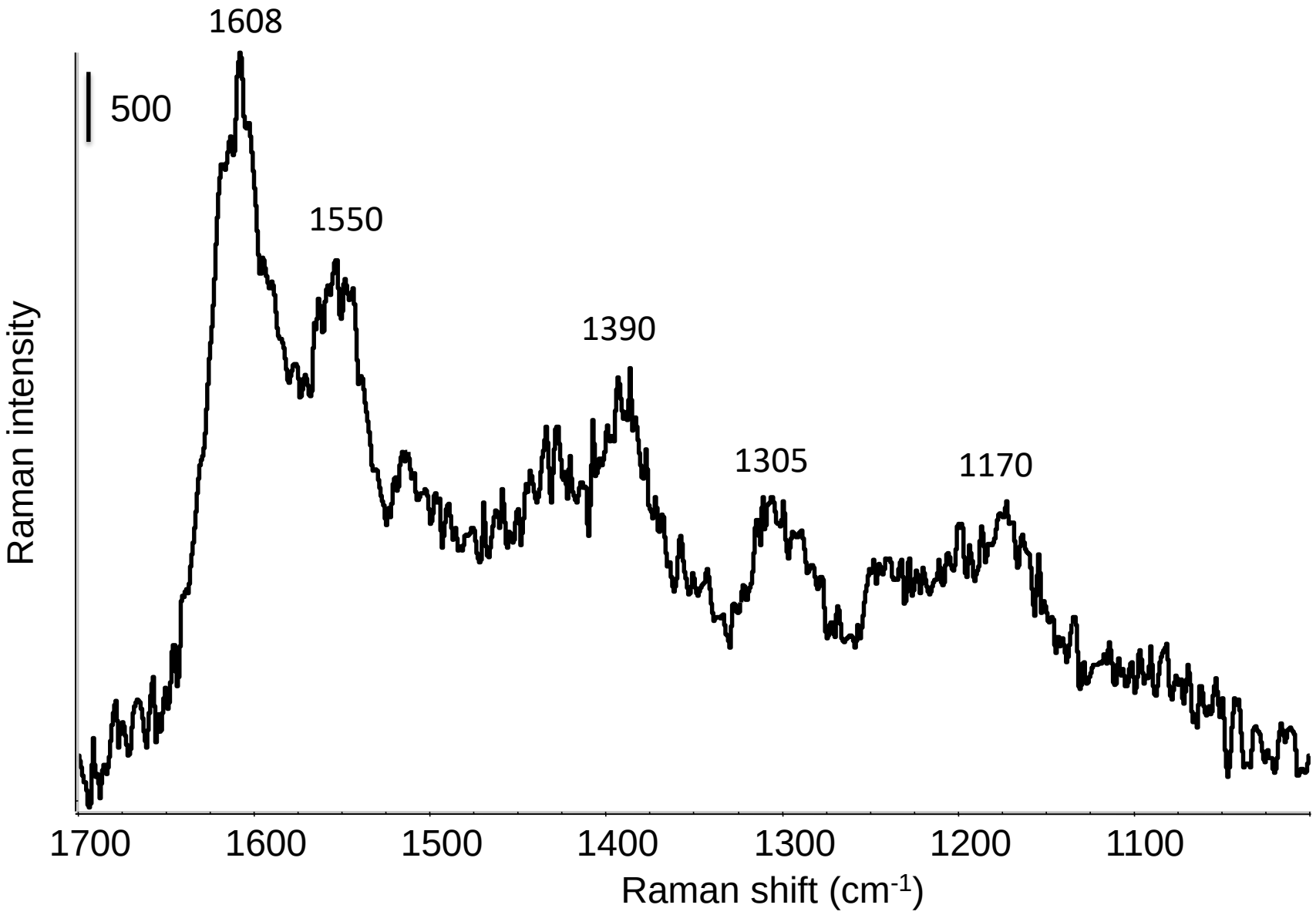
1608
500
1550
1390
1305
1170
Raman intensity
1700
1600
1500
1400
1300
1200
1100
Raman shift (cm-1)

Figure 11

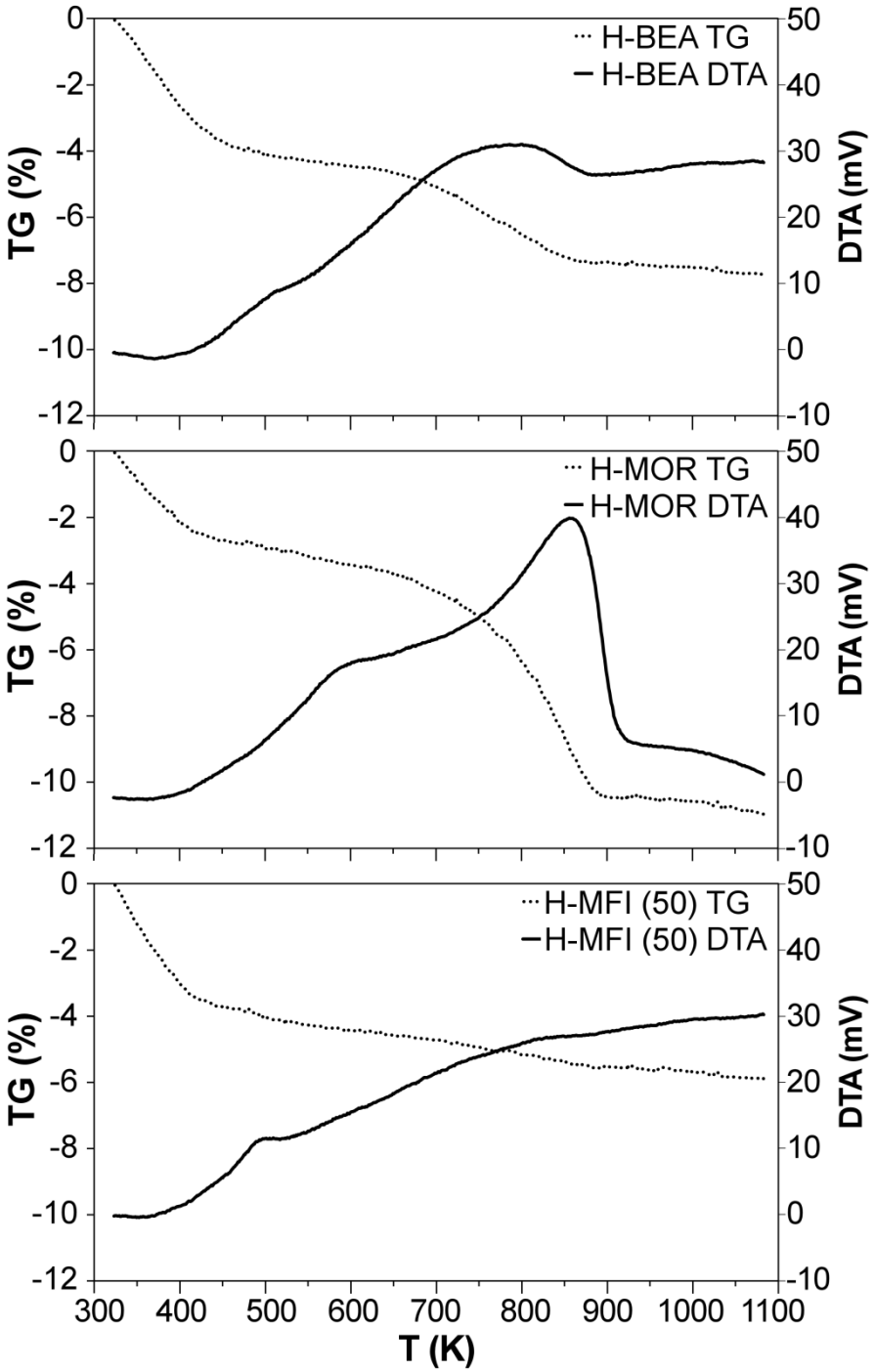
H-BEA TG
H-BEA DTA
H-MOR TG
H-MOR DTA
H-MFI (50) TG
H-MFI (50) DTA
TG (%)
DTA (mV)
T (K)
0
-2
-4
-6
-8
-10
-12
50
40
30
20
10
0
-10
300
400
500
600
700
800
900
1000
1100

Figure 12

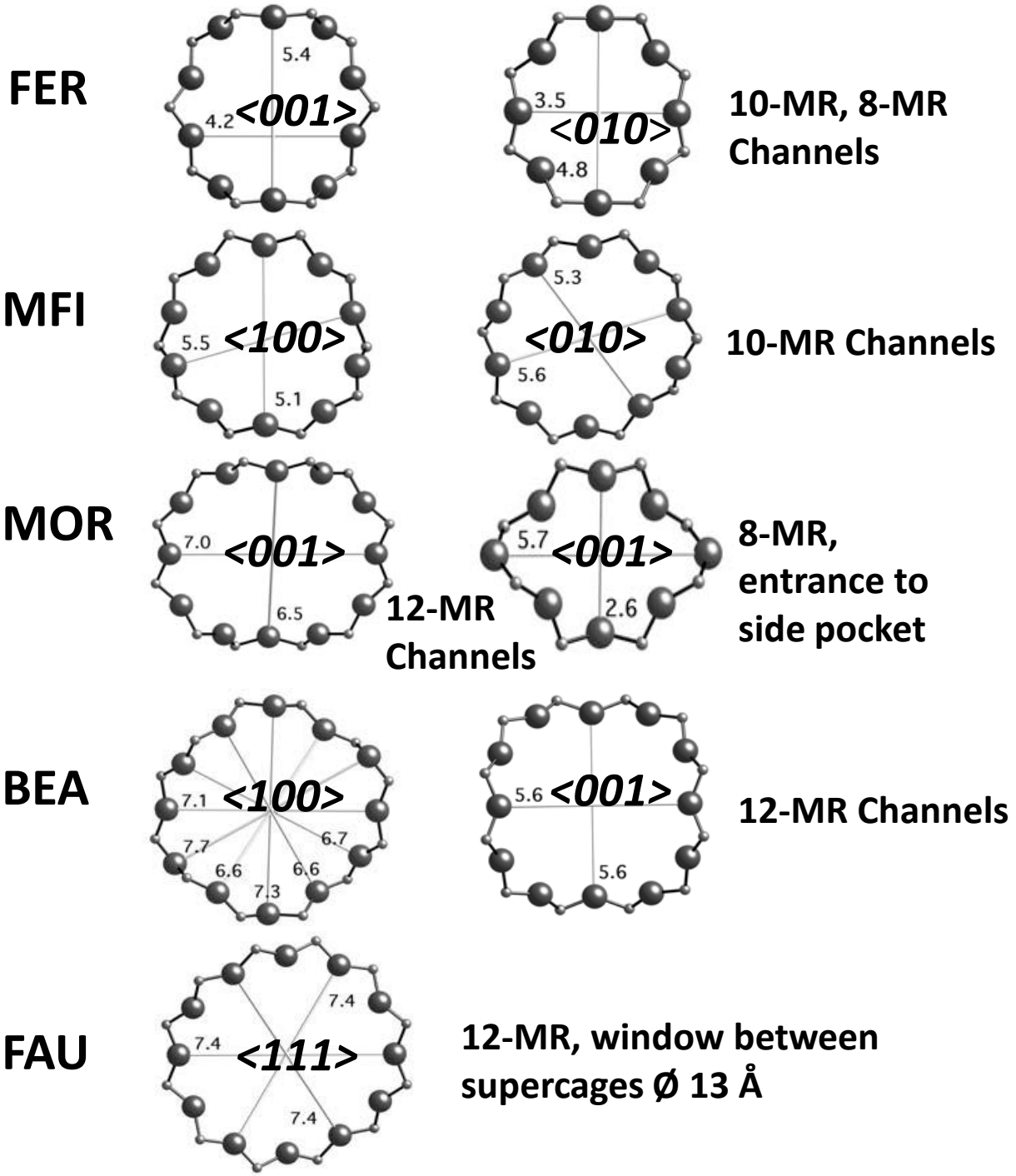
FER
5.4
4.2
<001>
3.5
<010>
4.8
10-MR, 8-MR Channels
MFI
5.5
<100>
5.1
5.3
<010>
5.6
10-MR Channels
MOR
7.0
<001>
6.5
12-MR Channels
5.7
<001>
2.6
8-MR, entrance to side pocket
BEA
7.1
<100>
7.7
6.7
6.6
6.6
7.3
5.6
<001>
5.6
12-MR Channels
FAU
7.4
7.4
<111>
7.4
12-MR, window between supercages Ø 13 Å